Natural Hazards (2019) 97:121–137
https://doi.org/10.1007/s11069-019-03630-3

ORIGINAL PAPER

A physically based spatiotemporal method of analyzing flood impacts on urban road networks

Yi Li[1,2,3] · Jianhua Gong[1,3] · Lei Niu[4] · Jun Sun[1,3]

Received: 25 August 2018 / Accepted: 25 May 2019 / Published online: 7 June 2019
© Springer Nature B.V. 2019

Abstract
Flash flooding occurs when low-lying geographic areas are rapidly flooded and is mainly caused by heavy rains. Urban road networks are the primary structures affected by flood inundation, which causes disruption to transportation and reduces the efficiency of rescue services. This paper proposes a physically based spatiotemporal method of analyzing flood impacts on urban road networks that considers both the physical parameters of flooding and the susceptibility of the transportation network. The results indicate that the proposed method provides reasonable spatiotemporal and synthetic estimates of impacts to the road network of Austin, Texas, USA, under flash flooding.

Keywords Flood disaster evaluation · Flash floods · Transportation network · Cellular automata

1 Introduction

Flash floods are considered one of the most devastating and deadly natural hazards in urban areas, and they are caused by an intense rain event that produces several hundreds of mm of rain in a few hours (Versini 2012). Recent studies have shown that flash floods are attracting growing public and research concern due to the increasing large-scale damage they cause in highly urbanized regions (Debionne et al. 2016, Vincendon et al. 2016, Pregnolato et al. 2017a). Urban road networks are among the critical infrastructure components that can be seriously affected by a flash flood due to their low-lying nature and high density throughout an urban territory (Yin et al. 2016). Inundation of urban road networks generally leads to high transportation vulnerability

✉ Jun Sun
sjunme@126.com

[1] State Key Laboratory of Remote Sensing Science, Institute of Remote Sensing and Digital Earth, Chinese Academy of Sciences, Beijing 100101, China

[2] Key Laboratory of Poyang Lake Wetland and Watershed Research, Ministry of Education, Jiangxi Normal University, Nanchang 330022, China

[3] Zhejiang-CAS Application Center for Geoinformatics, Jiashan 314100, Zhejiang, China

[4] School of Surveying Engineering, Henan University of Urban Construction, Pingdingshan 467036, China

and flood-related deaths as a result of vehicles being driven through flooded roadways (Jonkman and Kelman 2005).

According to the definition of "flood risk" used by the EU Flood European Floods Directive 2007/60/EC (EC 2007), we define the flood risk in a road network as the combination of the probability of a flood event and the potential adverse consequences for transport functions, security, society and economy when a road network is impacted by a flood event. The failure of a road network has the great impact on our daily lives as well as rescue operations for disasters. Therefore, a detailed analysis of flood hazards (characterized by the probability of flood events with a certain magnitude and other characteristics) and the flood vulnerability of road networks (considering the degree of influence on transportation at a given flood depth) should be performed to form a comprehensive understanding of the flood risks associated with road networks in urban areas.

Methods of assessing the hazards, risks and vulnerability associated with flooding can be categorized into two types (Balica et al. 2013): physically based methods (Hansson et al. 2008; Li et al. 2013) and parametric methods. The parametric approach is often used when only a few parameters are available but the goal is to estimate the complete vulnerability value of a system. Connor and Hiroki (2005) proposed a Flood Vulnerability Index (FVI), which combines different cause and effect factors and consists of four components (meteorological, hydrogeological, socioeconomic, and a countermeasure component) (Connor and Hiroki 2005; Balica et al. 2009). Although the parametric method can perform a wider evaluation of flood vulnerability, it does not provide a rigorous assessment of flood risk (Balica et al. 2013); moreover, it fails to explore the spatiotemporal characteristics of the flood vulnerability of residents during flash floods.

Physically based hydrological models and finite difference methods of hydraulic calculations (Ghimire et al. 2013; Li et al. 2015; Liu et al. 2015) have been used to estimate dynamic flood parameters that can be combined with social vulnerability data to understand disaster processes. Recent studies have performed evaluations of the flood impacts on road networks (Vincendon et al. 2016; Lang et al. 2016; Yin et al. 2016; Pedrozo-Acuña et al. 2017), flood hazard analyses for people and vehicles (Xia et al. 2011), assessments of the daily exposure of commuters (Terti et al. 2015; Debionne et al. 2016), and correlations between depth and disruption from economic aspects (Penning-Rowsell et al. 2013; Pregnolato et al. 2017b). This research has provided physically based analyses for the hazards, exposure or vulnerability associated with road network flooding. However, the current literature fails to integrate all these elements into a unified framework to provide the ability to perform spatiotemporal analyses and examine how flood dynamics affect people's transportation based on individual characteristics (e.g., income, age, and social relationships). Therefore, detailed information about the daily exposure of commuters to flooding (Debionne et al. 2016) and the risk factors for driving into flooded roads (Lim et al. 2016; Drobot et al. 2007) should also be considered via spatiotemporal analyses to achieve a comprehensive and synthetic understanding of flood impacts on road networks.

In this paper, we propose a physically based spatiotemporal method to analyze the impacts of floods on urban road networks. A Cellular Automata (CA) model is developed to address the spatiotemporal urban flood complexity, and the multiple transportation characteristics of stakeholders are incorporated to evaluate the dynamic impact of floods on urban road networks. The conclusions drawn in this work can identify mapped regions with high potential emergency management risks during a flash flood event.

2 Materials and methods

The case study area is located in the central part of the city of Austin (Town Lake-Colorado River sub-watershed area) in Texas, USA (Fig. 1). Austin is on the shore of the Colorado River and the 11th-most populous city in the USA. The elevation of Austin varies from 425 feet (130 m) to approximately 1000 feet (305 m) above sea level. Austin has experienced frequent flash floods, which are often caused by thunderstorms. The 2015 Halloween Flood was a presidentially declared disaster that affected Austin and Travis County and began during the pre-dawn hours of October 30, 2015 (Swearengin and Moore-Guajardo 2015).

2.1 Data availability and processing

This section introduces the data collection and processing methods. Our data sets include rainfall data, topography data, land use and soil data, and road network and commuting data.

2.1.1 Rainfall data

Rainfall is a disaster-inducing factor since it serves as an external driving force in the dynamic evolution of urban flooding. The historical precipitation in Austin can be obtained from the Weather Underground web site, which is a commercial weather service that provides real-time weather information via the Internet. To simulate the 2015 Halloween Flood in Austin, we downloaded the hourly historical precipitation data of October 30th, 2015. The data

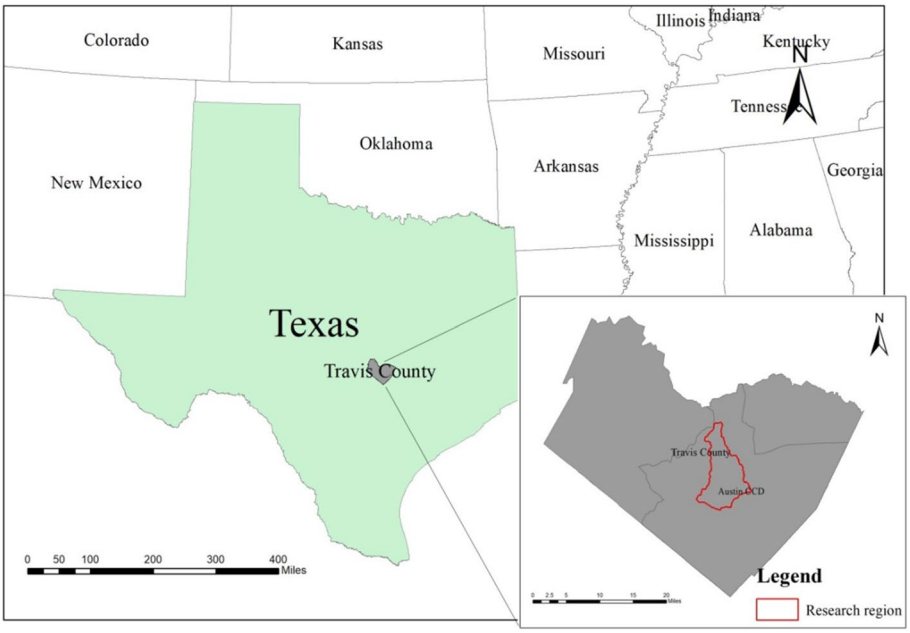

Fig. 1 Research area

were processed into rainfall data at a time scale of seconds as an input to the flood simulation model.

2.1.2 Topography data

Ten-meter resolution Digital Elevation Model (DEM) and gauge station data were acquired from the national map web site of the United States Geological Survey (https://viewer.nationalmap.gov/basic/) (Fig. 2a).

The hydrological characters of an urbanized area are affected by buildings. In this work, the building boundary data were obtained from the United States Census Bureau (https://www.census.gov/geo/maps-data/data/tiger-geodatabases.html); the GIS-based dataset provides characteristics that include the heights of each building polygon (Fig. 2b).

The Digital Surface Model (DSM) of the urban area is represented by overlay and raster calculation operations of the DEM layer and the building layer and rasterized using building height attributes.

2.1.3 Land use and soil type data

In this study, the surface roughness and infiltration factors in the research area could be empirically estimated using land use and soil types, which affect the rainfall-runoff and flood routine characteristics in flash floods. The land use data were downloaded from the Multi-Resolution Land Characteristics Consortium (MRLC) (https://www.mrlc.gov/nlcd11_data.php), and the soil type data were downloaded from the United States Department of Agriculture (https://www.nrcs.usda.gov/wps/portal/nrcs/detail/soils/survey/?cid=nrcs142p2_053627).

The runoff curve number method (United States Department of Agriculture 1986) was used to estimate the runoff factor from the simulated excess rate of rainfall:

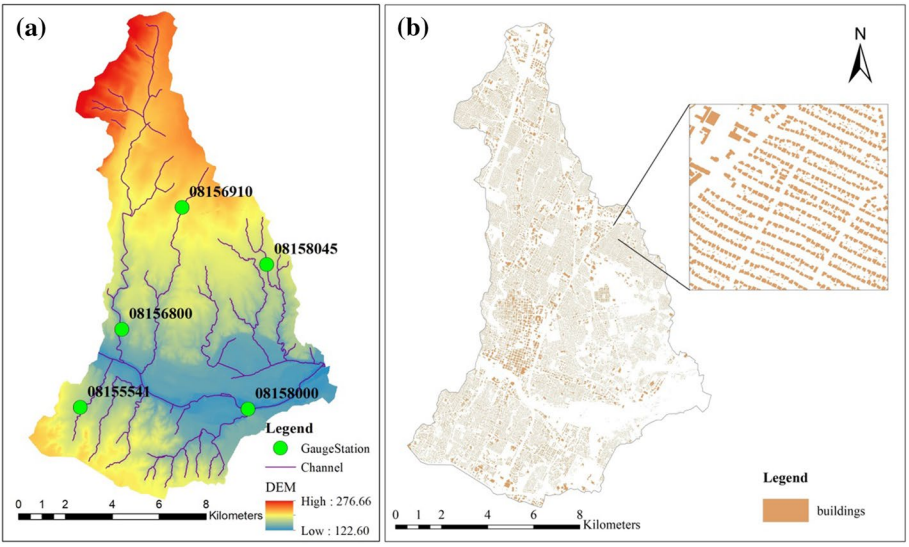

Fig. 2 Topological data

$$Q = \frac{\left(P - I_a\right)^2}{\left(P - I_a\right) + S} \tag{1}$$

where Q represents runoff (m), P represents rainfall (m), S represents potential maximum retention after runoff begins (m) and I_a represents the initial abstraction (m). For urbanized watersheds, we adopt $I_a = 0.05S$ (Hawkins et al. 2002), and

$$S = \left(\frac{1000}{\mathrm{CN}} - 10\right) \Big/ 39.37 \tag{2}$$

where CN represents the runoff curve number, which ranges from 30 to 100 and was extracted from the land use classification and soil type data (United States Department of Agriculture 1986).

2.1.4 Road network and commuting data

The commuting statistical data at the district level are more accessible than individual travel trajectories due to privacy issues. The exposure analysis of commuters during flash floods should consider the distribution of road network and the time-varying commuting statistics. In the research area, the hourly statistical commuting statistic data at the district level can be obtained from the United States Census Bureau. In addition, the distribution of travel time to work in districts is also documented in the dataset, which can assist in the collection of statistics of the averaged travel time in each district.

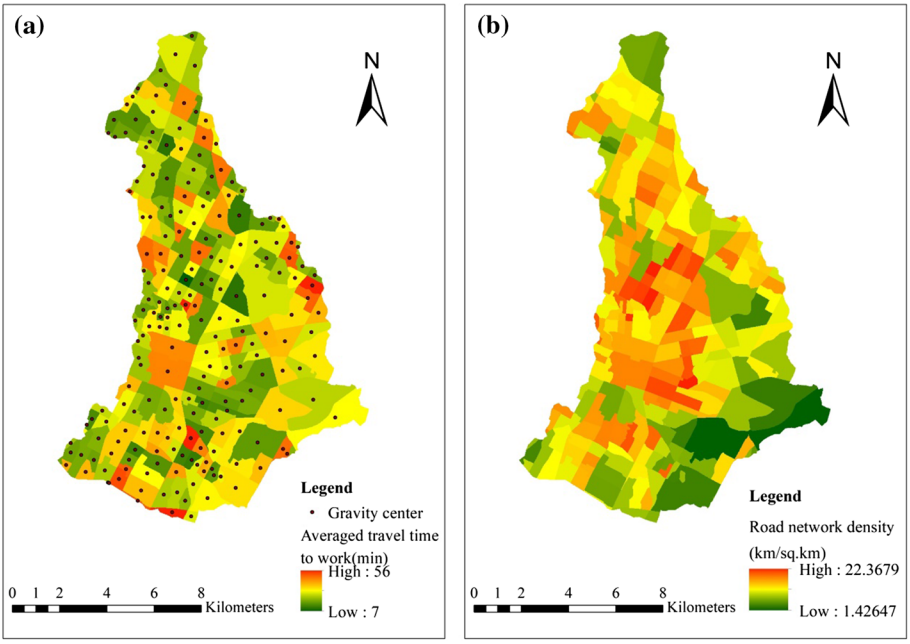

Fig. 3 Road network and commuting statistics for the **a** average travel time to work and **b** road density

Figure 3a depicts the 213 district partitions, where gravity centers are represented as black dots on the map. Figure 3b illustrates the road network density in each district.

2.2 Methods

This section introduces a group of methods that were developed for this research work. The methods include a cellular automata model for urban flood simulation and a road network impact analysis method based on the spatiotemporal flood simulation results.

2.2.1 Cellular automata model for urban flood simulation

In this work, we developed a cellular automata model for analyzing flood impacts on road networks in the city of Austin. A proposed cellular automata model (Fig. 4) for road network inundation impact simulations includes two stages: cellular automata initialization and cellular automata simulation. The cellular automata model is initialized by preparing all the data layers under a unified grid size and boundary. A Von Neumann neighborhood structure is adopted to carry out the simulations for road network inundation impact analysis.

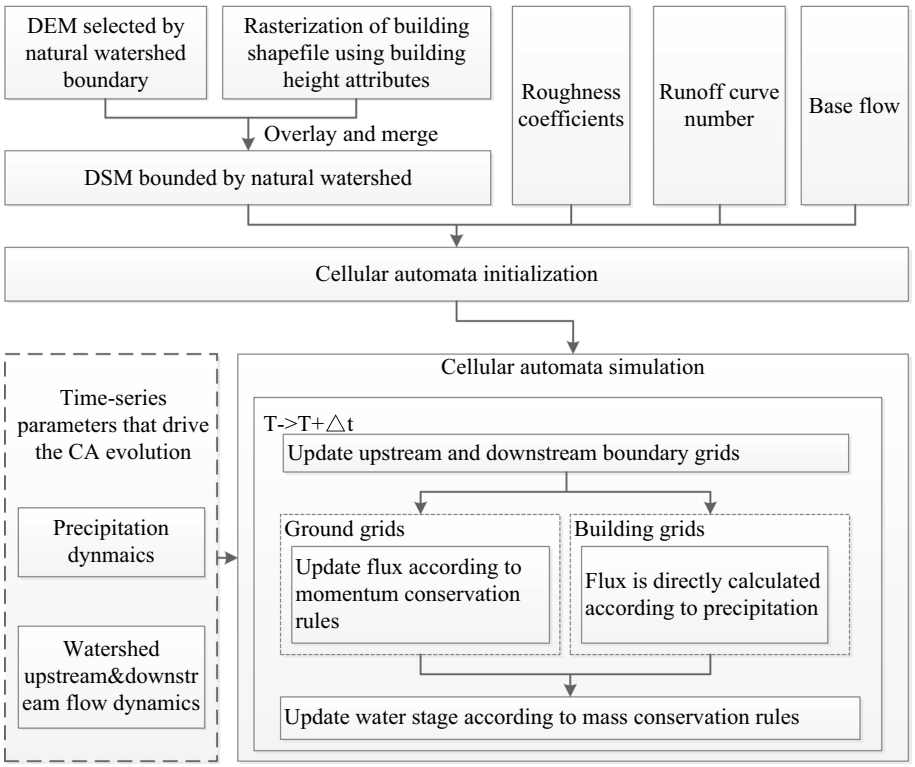

Fig. 4 Cellular automata model for urban flood simulation

The simulation of an urban flash flood has three key characters: (1) it is mainly driven by intensive precipitation in a short period; (2) the impact of buildings on the watershed landform and flood routine should be considered at an appropriate level of detail; and (3) the infiltration and drainage parameters are specified on spatial and temporal discrete grids.

In this article, an effective flood modeling and simulation workflow appropriate for catchments mainly occupied by buildings is proposed. The dynamic precipitation data of each step are obtained by interpolation of the weather observations and added to the water stage of each grid cell (the grid cells taken up by buildings are treated in the same way).

The movement of water volume among non-building cells is solved by shadow water equations fitted in a cellular automation framework as introduced by Li et al. (2013):

$$M_{i,j}^{t+1} = M_{i,j}^{t} - g\frac{\Delta t(h_{i+1,j}^{t} + h_{i,j}^{t})(z_{i+1,j}^{t} - z_{i,j}^{t})}{\Delta x} - gn_{i,j}^{2}\frac{\overline{u}_{i,j}\Delta t\sqrt{\left(u_{i,j}^{t}\right)^{2} + \left(v_{i,j}^{t}\right)^{2}}}{\left[(h_{i+1,j}^{t} + h_{i,j}^{t})/2\right]^{1/3}} \tag{3}$$

$$N_{i,j}^{t+1} = N_{i,j}^{t} - g\frac{\Delta t(h_{i,j+1}^{t} + h_{i,j}^{t})(z_{i,j+1}^{t} - z_{i,j}^{t})}{\Delta y} - gn_{i,j}^{2}\frac{\overline{v}_{i,j}\Delta t\sqrt{\left(u_{i,j}^{t}\right)^{2} + \left(v_{i,j}^{t}\right)^{2}}}{\left[(h_{i,j+1}^{t} + h_{i,j}^{t})/2\right]^{1/3}} \tag{4}$$

$$h_{i,j}^{t+1} = h_{i,j}^{t} - \frac{\Delta t(M_{i+1,j}^{t+1} - M_{i,j}^{t+1})}{\Delta x} - \frac{\Delta t(N_{i,j+1}^{t+1} - N_{i,j}^{t+1})}{\Delta y} + Q_{i,j}^{t} - EV_{i,j}^{t} \tag{5}$$

In Eqs. (3)–(5), $h_{i,j}^{t}$ represents the average water depth (m) of the CA cell (i, j) at time t; $M_{i,j}^{t}$ and $N_{i,j}^{t}$ are the single-width fluxes ($m^2\ s^{-1}$) of the CA cell (i, j) at time t in the x and y directions, respectively; $\mu_{i,j}^{t}$ and $v_{i,j}^{t}$ represent the average horizontal water speeds ($m\ s^{-1}$) in the CA cell (i, j) at time t in the x and y directions, respectively, where $\mu_{i,j}^{t} = M_{i,j}^{t}/h_{i,j}^{t}$ and $v_{i,j}^{t} = N_{i,j}^{t}/h_{i,j}^{t}$; $z_{i,j}^{t}$ represents the average water stages (m) of the CA cell (i, j) at time t; $Q_{i,j}^{t}$ is the estimated runoff value ($m\ s^{-1}$) of the CA cell (i, j) obtained from formulas (1), (2); $EV_{i,j}^{t}$ is the evaporation value (omitted for flash flood analysis); $n_{i,j}$ is the hydraulic roughness coefficient ($m^{-1/3}\ s$) of the CA cell (i, j); and Δt, Δx, and Δy represent the temporal unit(s), the spatial unit in the x direction (m), and the spatial unit (m) in the y direction, respectively.

The calculations of water volume movement from building cells to non-building cells need to be adjusted due to significant elevation differences as shown in Fig. 5.

The water flux through the four neighborhoods of grid (i, j) can be calculated with Eqs. (3) and (4), where $M_{i,j}^{t}$ and $N_{i,j}^{t}$ are the single-width fluxes ($m^2\ s^{-1}$) of the CA cell (i, j) at time $T+\Delta t$ in the x and y directions, respectively; P^T is the precipitation intensity ($m\ s^{-1}$); $NE_{i,j}$ is the number of edges of grid(i, j) that are adjacent to ground grids; and Δt, Δx, and Δy represent the temporal unit(s), the spatial unit in the x direction (m), and the spatial unit (m) in the y direction, respectively.

$$M_{i,j}^{T+\Delta t} = -M_{i,j-1}^{T+\Delta t} = \frac{P^T \times \Delta x}{NE_{i,j}} \tag{6}$$

$$N_{i,j}^{T+\Delta t} = -N_{i-1,j}^{T+\Delta t} = \frac{P^T \times \Delta y}{NE_{i,j}} \tag{7}$$

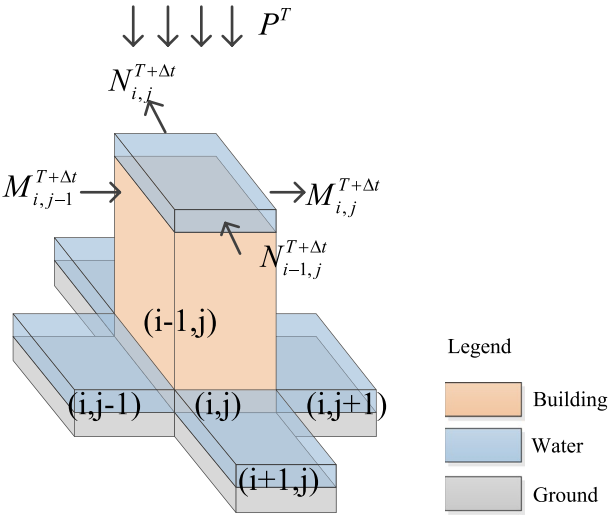

Fig. 5 Calculations of water volume movement from building cells to non-building cells

2.2.2 Spatial–temporal road network impact analysis method

For most studies in flash flood risk analysis, human mobility is rarely considered and residential population density data are usually assumed to have a static distribution (Debionne et al. 2016). This paper adopts a dataset that collects statistical data on hourly variations of commuting behavior that can be integrated with flash flood dynamic data to provide a more accurate and appropriate spatiotemporal commuter exposure analysis for flash floods.

The proposed estimation method is based on two assumptions: (1) for each district, the commuters are distributed with equal spatial probability in each road cell and equal temporal probability in each time span (as was documented in the statistical data); and (2) each commuter travels using the averaged commuting time of the district in which he or she lives. The detailed transition rules for the flood exposure of commuters at each road cell are depicted in Fig. 6.

Equations (8) and (9) demonstrate the calculation method of CE_i^t(commuter exposure estimation of road cell i at time t) (person s^{-1}):

$$CE_i^t = DC_c^t \times R_c \Big/ (V_{\text{moter}} \times NRG_c) + \sum_{0 \le j < n\text{Dist}}^{j \ne c} CE_{j->i}^t \tag{8}$$

$$\text{CE}_{j->i}^t = \begin{cases} \dfrac{\text{DC}_j \Big/ {}_{t-} d_j^i \Big/ V_{\text{moter}} \times \Delta x \Delta y}{\pi d_j^{i2} \times \text{NRG}_{\text{Total}} / \text{NG}_{\text{Total}}} & \left(\text{if} \quad d_j^i \Big/ V_{\text{moter}} \le \text{CT}_j\right) \\ 0 & \left(\text{if} \quad d_j^i \Big/ V_{\text{moter}} \le \text{CT}_j\right) \end{cases} \tag{9}$$

where DC_c^t represent the number of commuters (person s^{-1}) in the current district of cell i at time t; nDist, $\text{NRG}_{\text{Total}}$ and NG_{Total} represent the number of districts, road grids and total CA grids in the research area, respectively; R_c and NRG_c represent the equivalent radius

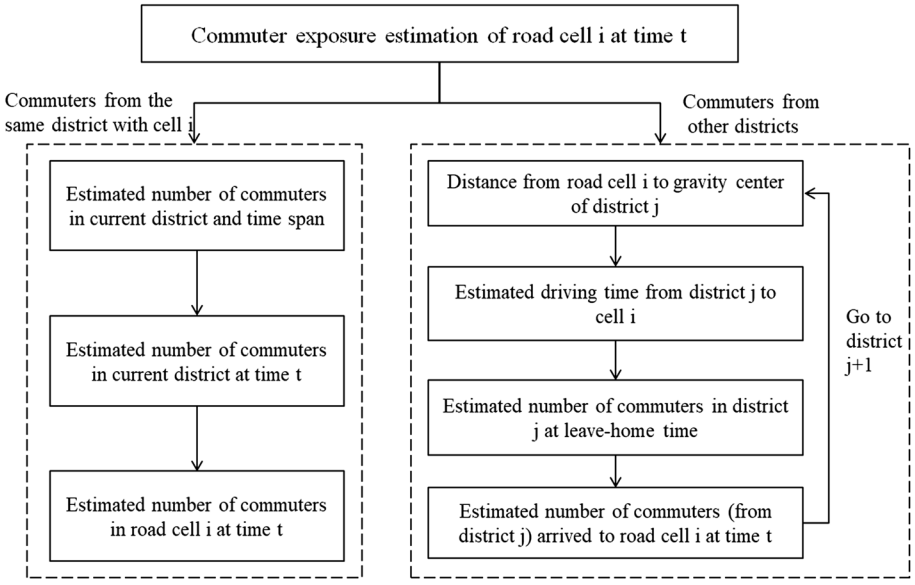

Fig. 6 Transition rules for the flood exposure estimation of commuters

(calculated according to the district area) and the number of road grids of the current district, respectively; d_j^i is the distance (m) from road cell i to the gravity center of district j, and V_{moter} is the estimated driving velocity (m s^{-1}); CT_j is the averaged commuting time (s) in district j; and Δx, Δy represent the spatial unit in the x and y direction (m), respectively. Therefore, $DC_j^{t-d_j^i/V_{\text{moter}}}$ represents the number of commuters in district j at leave-home time and $\sum_{0\le j<n\text{Dist}}^{j\neq c} CE_{j->i}^t$ is the estimation of commuter exposure of road cell i at time t contributed by other districts.

For the road network impact analysis, the flood depth needs to be translated via the road network into increased commuting time and then evaluated using the value of time (VoT) (Ford et al. 2015). Pregnolato et al. (2017b) proposed a relationship between flood water and vehicle speed that has proven to be a good fit to the observed data and has an R-square value of 0.95:

$$v(h) = 0.0009h^2 - 0.5529h + 86.9448 \tag{10}$$

where v represents the vehicle speed limit (km/h) and h is the flood depth (mm).

In this paper, we adopt the relationship to estimate the vehicle speed reduction due to flooding. Therefore, the total road network impact at time t (RD(t)) can be calculated by Eq. (11):

$$\text{RD}(t) = \sum_{i\in S} \text{CE}_i^t \times \left(1 - {}^{v(h_i^t)}/_{v_0}\right) \times VoT \tag{11}$$

where CE_i^t represents the commuter exposure estimation of road cell i at time t (person s^{-1}) introduced in Eqs. (8) and (9); $v(h_i^t)$ is the maximum speed as a function of flood depth in cell i at time t; v_0 is the speed allowed by transport regulations; and VoT is the value of

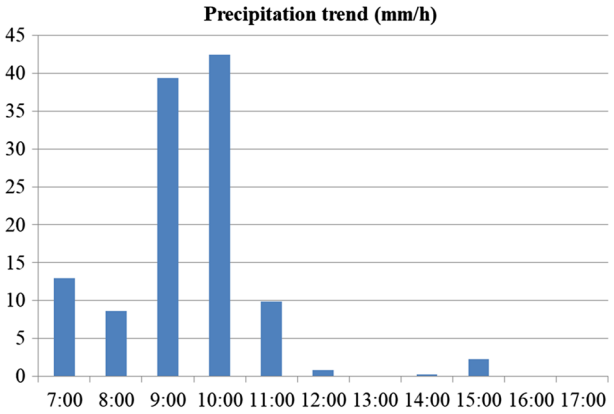

Fig. 7 Precipitation trend in study area from 7:00 to 17:00 on October 30th, 2015

Table 1 Submerged statistics (sq.km)

Water depth (m)	Time					
	7:30	9:00	10:00	11:00	13:00	17:00
0–0.3	126.92	126.43	122.7	118.04	116.82	117.48
0.3–1	0.46	0.91	4.32	8.05	8.58	8.11
1–3	1.92	1.68	1.95	2.82	3.33	2.88
3–10	0.3	0.58	0.63	0.69	0.87	1.13

time (dollar s^{-1}). The *VoT* value used in this paper was based on US average hourly wages, which were US$ 21.19 per hour (in Oct. 2015 prices).

3 Results

The CA model was initialized using the DSM, roughness coefficient, infiltration, and population density datasets. A profile of precipitation from 7:00 to 17:00 on October 30th, 2015 is shown in Fig. 7. The water flux through the segment of the Colorado River that connects the upstream and downstream of the sub-watershed was estimated from the 5-minute-interval observational data of gauge station 08158000 and preprocessed to fit into the CA model together with the precipitation time-series data.

The cellular automata model was used for a simulation from 7:00 to 17:00. Here, we choose 6 moments of time to illustrate the dynamic change of the water depth. The submerged statistics, broken down by graded water depth, are shown in Table 1. Figure 8 is also provided to depict the evolution of flood, which illustrates that dramatic streams and ponds quickly form in the urban area from 9:00 to 11:00 and gradually recede after 13:00. The grades of water depth are selected manually, in which 0.3 meters is important because it is usually the height of the exhaust pipe of a vehicle. Other grades are selected to carry out appropriate spatiotemporal flood mapping in the study area.

The simulated results of commuter exposure are shown in Fig. 9 and estimated according to the methods in Sect. 2.2.2. The results indicate that the estimated numbers of commuters exposed in the road network at 7:30, 9:00 and 10:00 are relatively higher than those

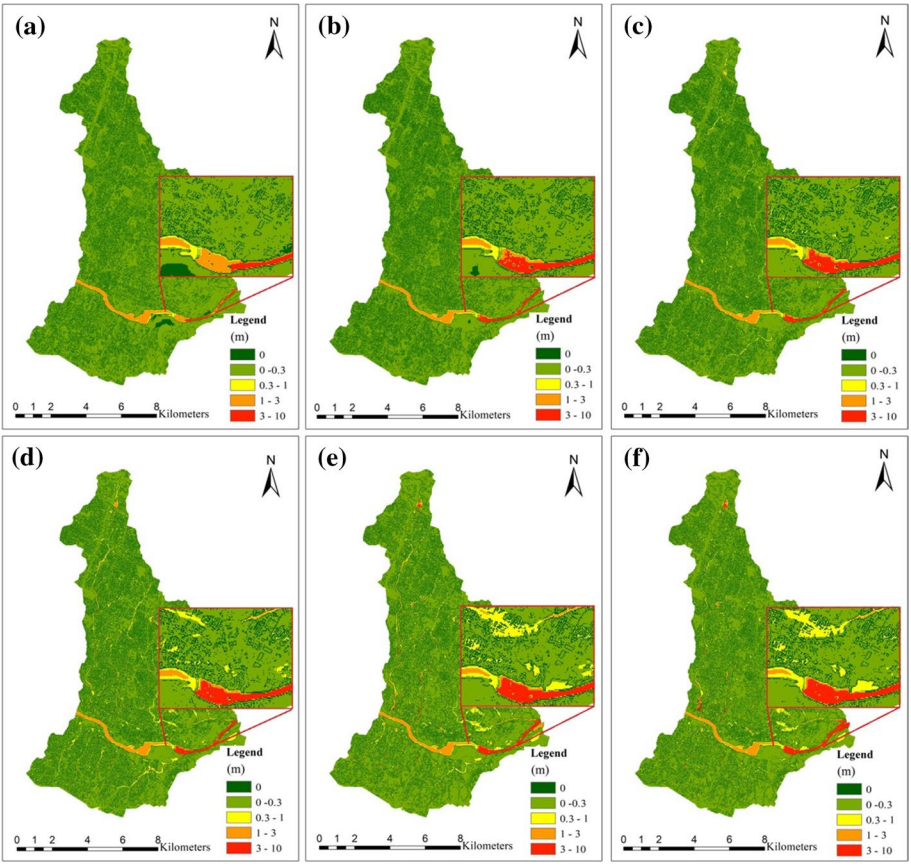

Fig. 8 Water depth results at time **a** 7:30, **b** 9:00, **c** 10:00, **d** 11:00, **e** 13:00, and **f** 17:00

after 10:00 because a number of commuters are still in the morning rush hour during that time.

The road network impact results were obtained via simulations, and the average road impact per CA grid in each district is shown in Fig. 10 to better describe the spatial and temporal patterns of road network impacts. Figure 10a–f shows that road network transportation is more affected at 7:30 and 10:00 than at other time nodes. For the analysis result at 7:30, the road impact peak is mainly formed by the morning rush hour according to the estimated commuter exposure in Fig. 10a, whereas the road impact peak at 10:00 is due to the joint effect of rainfall-runoff and urban commuting dynamics. A rainfall peak from 9:00 to 10:00 results in a dramatic increase in the waterlogging depth, and the highly affected districts at 10:00 are mainly distributed around the shore of the Colorado River (see Fig. 10c). We can conclude that the CA model provides a spatiotemporal estimation of commuter distribution that can unite the spatiotemporal calculation of flood parameters and offer insights from the road network impact analysis.

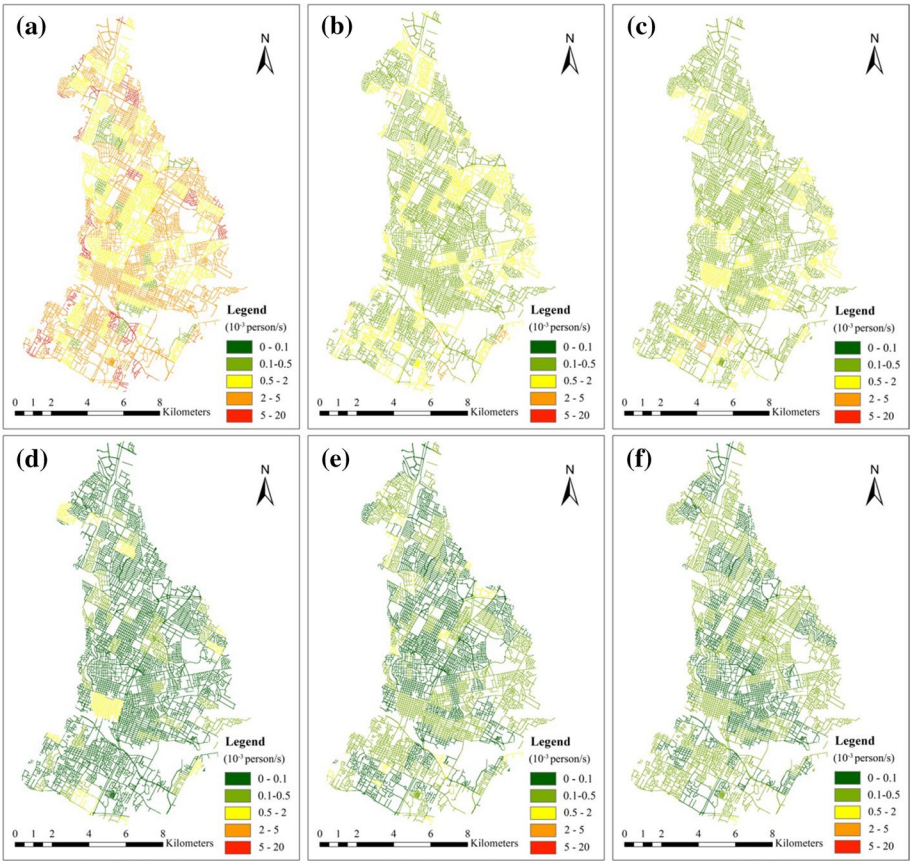

Fig. 9 Estimated commuter exposure at time **a** 7:30, **b** 9:00, **c** 10:00, **d** 11:00, **e** 13:00, and **f** 17:00

4 Discussion

In this paper, we validated the performance of urban flood inundation simulation by comparisons with the time-series observation data from four gauge stations (Fig. 11). The simulated hydrographs can reflect the dynamic trend of flood evolution, which can provide spatiotemporal datasets for a road network impact analysis.

We also investigated a parametric approach (Flood Vulnerability Index (FVI)) to provide comparisons with the proposed physically based spatiotemporal method. Table 2 illustrates the flood vulnerability index designations.

The FVI method can only provide a vulnerability result between 0 and 1. Spatial and temporal results such as economic loss cannot be achieved by this parametric method. A summarization was further provided (Table 3) among the proposed methods, parametric approaches (such as FVI) and traditional physically based hydraulic modeling.

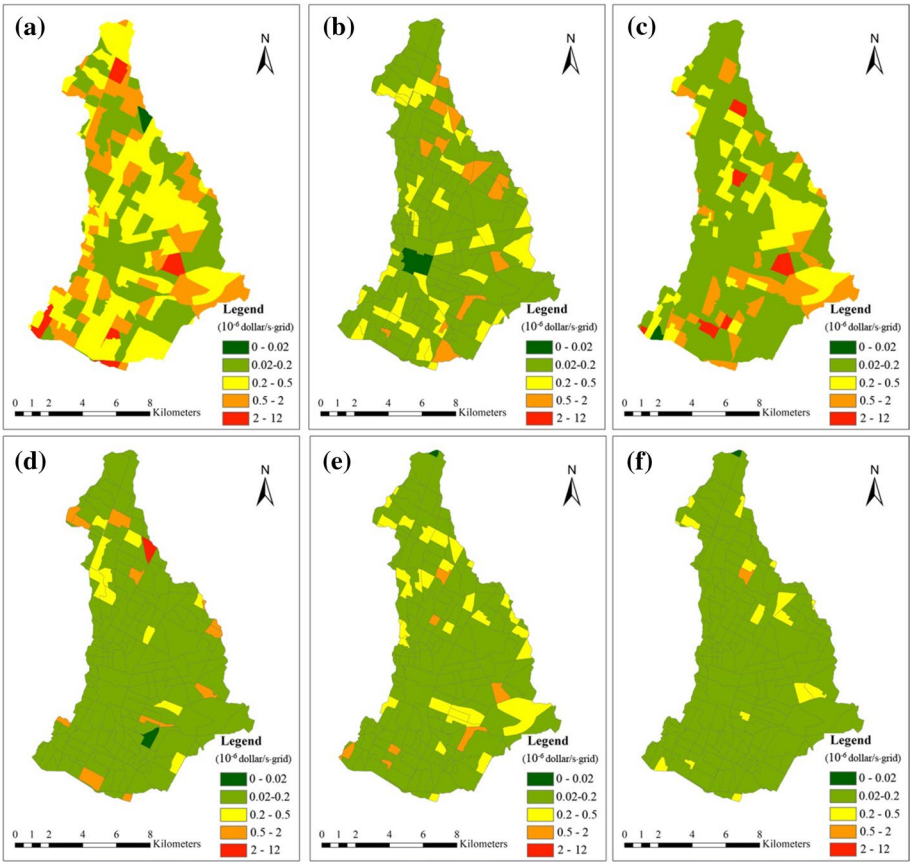

Fig. 10 District-averaged road network impact estimated at time **a** 7:30, **b** 9:00, **c** 10:00, **d** 11:00, **e** 13:00, and **f** 17:00

We can conclude that the proposed physically based method inherits the advantage of traditional physically based methods in which the phenomena of river flow and flooding can be quantitatively described by coupled sets of equations. Moreover, the proposed method extends to flood vulnerability elements and thus provides quantitative economic loss estimations in flood events.

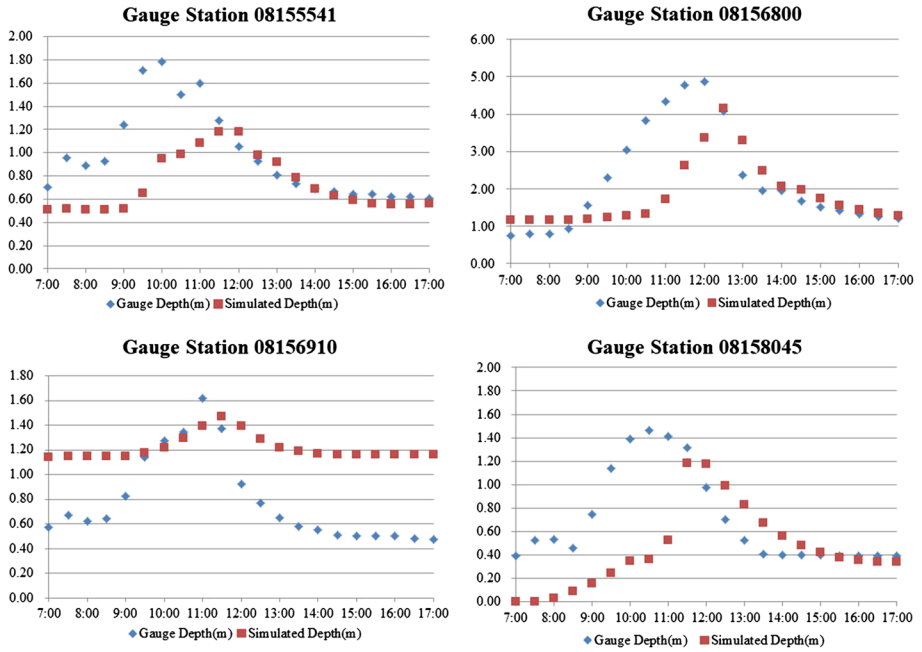

Fig. 11 Comparisons between gauge depth and simulated water depth

5 Conclusions

A fully dynamic simulation analysis of flood impacts on urban road networks is a challenging and meaningful task: it is challenging because the flood impacts on road networks represent interactions among hazards, exposures, and risk vulnerabilities, which makes it rather complex to explore and validate all the elements; and it is meaningful in that it provides insights into and knowledge of the comprehensive spatiotemporal information of the flood process.

In this research work, we combined flood rainfall-runoff simulations and commuting exposure estimations at a spatiotemporally discrete level and a VoT-based vulnerability analysis was developed to fit in the cellular automata analysis. Our proposed method enabled a quantitative spatiotemporal road network impact analysis for flash floods. From the analysis results, the evolution of a flood and its impact on a road network could be visualized, including spatial details.

In this paper, the district-level commuting behavior data are based on a statistical approach. However, a more comprehensive model could be achieved if more detailed commuting data are obtained. In addition, we considered the infiltration effect during the rainfall-runoff process using an empirical method that estimated the runoff curve number. Errors exist because detailed urban drainage pipeline data and accurate landform and rainfall distributions are difficult to obtain, which also reflects the limitations of physically based modeling techniques.

Table 2 Flood vulnerability designations of road network

Designation	Index value	Description
Very small vulnerability to floods	< 0.01	Very small vulnerability to floods, very low number of commuters and road grids, very small proportion of impervious layer
Small vulnerability to floods	0.01–0.25	Small vulnerability to floods, low number of commuters and road grids, small proportion of impervious layer
Vulnerable to floods	0.25–0.50	Vulnerable to floods, medium number of commuters and road grids, medium proportion of impervious layer.
High Vulnerability to floods	0.50–0.75	High vulnerability to floods, high number of commuters and road grids, high proportion of impervious layer
Very high vulnerability to floods	0.75–1	Very high vulnerability to floods, very high number of commuters and road grids, very high proportion of impervious layer

Table 3 Method comparisons

	Fully dynamic process	Quantitative flood calculations	Consideration of commuting exposure	Quantitative economic loss calculations
Proposed methods	Yes	Yes	Yes	Yes
Flood vulnerability index methods	No	No	Yes	No
Traditional physically based hydraulic methods	Yes	Yes	No	No

Acknowledgements This research is supported by the Strategic Priority Research Program of Chinese Academy of Sciences (Grant No. XDA 20030302); the National Natural Science Foundation of China (41471341, 41871323, 41771433); the Opening Fund of Key Laboratory of Poyang Lake Wetland and Watershed Research (Jiangxi Normal University), Ministry of Education (PK2016002).

References

Balica SF, Douben N, Wright NG (2009) Flood vulnerability indices at varying spatial scales. Water Sci Technol 60:2571–2580

Balica S, Popescu I, Beevers L, Wright NG (2013) Parametric and physically based modelling techniques for flood risk and vulnerability assessment: a comparison. Environ Model Softw 41:84–92

Connor R, Hiroki K (2005) Development of a method for assessing flood vulnerability. Water Sci Technol 51:61–67

Debionne S, Ruin I, Shabou S, Lutoff C, Creutin J-D (2016) Assessment of commuters' daily exposure to flash flooding over the roads of the Gard region, France. J Hydrol 541:636–648

Drobot SD, Benight C, Gruntfest E (2007) Risk factors for driving into flooded roads. Environ Hazards 7:227–234

European Floods Directive (2007) L 288/27, Official Journal of the European Union, Brussels

Ford A, Barr S, Dawson R, James P (2015) Transport accessibility analysis using GIS: Assessing sustainable transport in London. ISPRS Int J Geo-Inform 4(1):124–149

Ghimire B, Chen AS, Guidolin M, Keedwell EC, Djordjević S, Savić DA (2013) Formulation of a fast 2D urban pluvial flood model using a cellular automata approach. J Hydroinform 15:676

Hansson K, Danielson M, Ekenberg L (2008) A framework for evaluation of flood management strategies. J Environ Manag 86(3):465–480

Hawkins RH, Jiang R, Woodward DE, Hjelmfelt AT, Van Mullem JA, (2002) Runoff curve number method: examination of the initial abstraction ratio. In: Proceedings of the second federal interagency hydrologic modeling conference, Las Vegas, Nevada. U.S. Geological Survey. https://doi.org/10.1111/j.1752-1688.2006.tb04481.x

Jonkman SN, Kelman I (2005) An analysis of the causes and circumstances of flood disaster deaths. Disasters 29:75–97

Lang M, Pregnolato M, Ford A, Dawson R, Klijn F, Samuels P (2016) Disruption and adaptation of urban transport networks from flooding. E3S Web of Conferences, 7, 07006

Li Y, Gong J, Zhu J, Song Y, Hu Y, Ye L (2013) Spatiotemporal simulation and risk analysis of dam-break flooding based on cellular automata. Int J Geogr Inf Sci 27:2043–2059

Li Y, Gong J, Liu H, Zhu J, Song Y, Liang J (2015) Real-time flood simulations using CA model driven by dynamic observation data. Int J Geogr Inf Sci 29:523–535

Lim HR, Lim MBB, Piantanakulchai M (2016) Determinants of household flood evacuation mode choice in a developing country. Nat Hazards 84:507–532

Liu L, Liu Y, Wang X, Yu D, Liu K, Huang H, Hu G (2015) Developing an effective 2-D urban flood inundation model for city emergency management based on cellular automata. Nat Hazards Earth Syst Sci 15:381–391

Pedrozo-Acuña A, Moreno G, Mejía-Estrada P, Paredes-Victoria P, Breña-Naranjo JA, Meza C (2017) Integrated approach to determine highway flooding and critical points of drainage. Transp Res Part D Transp Environ 50:182–191

Penning-Rowsell E, Priest S, Parker D, Morris J, Tunstall S, Viavattene C, Chatterton J, Owen D (2013) Flood and coastal erosion risk management: a manual for economic appraisal. Routledge, Abingdon

Pregnolato M, Ford A, Glenis V, Wilkinson S, Dawson R (2017a) Impact of climate change on disruption to urban transport networks from pluvial flooding. J Infrastruct Syst 23:04017015

Pregnolato M, Ford A, Wilkinson SM, Dawson RJ (2017b) The impact of flooding on road transport: a depth-disruption function. Transp Res Part D Transp Environ 55:67–81

Swearengin RS, Moore-Guajardo S (2015) Halloween flood October 30, 2015. City of Austin and Travis County After Action Report. http://www.austintexas.gov/sites/default/files/files/hsem/2015_Halloween_Flood_AAR_City-County_Final.pdf. Accessed 25 May 2018

Terti G, Ruin I, Anquetin S, Gourley JJ (2015) Dynamic vulnerability factors for impact-based flash flood prediction. Nat Hazards 79:1481–1497

United States Department of Agriculture,1986. Urban hydrology for small watersheds. Technical Release 55 (TR-55) (Second ed.). Natural Resources Conservation Service, Conservation Engineering Division

Versini P-A (2012) Use of radar rainfall estimates and forecasts to prevent flash flood in real time by using a road inundation warning system. J Hydrol 416–417:157–170

Vincendon B, douard S, Dewaele H, Ducrocq V, Lespinas F, Delrieu G, Anquetin S (2016) Modeling flash floods in southern France for road management purposes. J Hydrol 541:190–205

Weather Underground (2015) Weather History for KATT-October, 2015. https://www.wunderground.com/history/airport/KATT/2015/10/30/DailyHistory.html. Assessed 21 June 2018

Xia J, Falconer RA, Lin B, Tan G (2011) Numerical assessment of flood hazard risk to people and vehicles in flash floods. Environ Model Softw 26:987–998

Yin J, Yu D, Yin Z, Liu M, He Q (2016) Evaluating the impact and risk of pluvial flash flood on intra-urban road network: a case study in the city center of Shanghai, China. J Hydrol 537:138–145

Publisher's Note Springer Nature remains neutral with regard to jurisdictional claims in published maps and institutional affiliations.